Time-resolved ion velocity distribution in a cylindrical Hall thruster: Heterodyne-based experiment and modeling

A. Diallo, S. Keller, Y. Shi, Y. Raitses, and S. Mazouffre

Articles you may be interested in

Unexpected transverse velocity component of Xe + ions near the exit plane of a Hall thruster
Phys. Plasmas **17**, 113502 (2010); 10.1063/1.3507308

A time-resolved laser induced fluorescence study on the ion velocity distribution function in a Hall thruster after a fast current disruption
Phys. Plasmas **16**, 043504 (2009); 10.1063/1.3112704

Electron cross-field transport in a low power cylindrical Hall thruster
Phys. Plasmas **11**, 4922 (2004); 10.1063/1.1791639

On the potential distribution in Hall thrusters
Appl. Phys. Lett. **85**, 2481 (2004); 10.1063/1.1797555

Electron density and energy distribution function in the plume of a Hall-type thruster
Rev. Sci. Instrum. **73**, 931 (2002); 10.1063/1.1431404

Time-resolved ion velocity distribution in a cylindrical Hall thruster: Heterodyne-based experiment and modeling

A. Diallo,[1] S. Keller,[1] Y. Shi,[1] Y. Raitses,[1] and S. Mazouffre[2]
[1]*Princeton Plasma Physics Laboratory, Princeton, New Jersey 08540, USA*
[2]*CNRS, ICARE, Orléans, France*

Time-resolved variations of the ion velocity distribution function (IVDF) are measured in the cylindrical Hall thruster using a novel heterodyne method based on the laser-induced fluorescence technique. This method consists in inducing modulations of the discharge plasma at frequencies that enable the coupling to the breathing mode. Using a harmonic decomposition of the IVDF, one can extract each harmonic component of the IVDF from which the time-resolved IVDF is reconstructed. In addition, simulations have been performed assuming a sloshing of the IVDF during the modulation that show agreement between the simulated and measured first order perturbation of the IVDF. © 2015 AIP Publishing LLC. [http://dx.doi.org/10.1063/1.4914829]

I. INTRODUCTION

Hall thrusters are key players in space electric propulsion and have been used to maintain and transfer orbits of satellites.[1] The cylindrical Hall thruster (CHT) is a type of Hall thruster designed for low power operations.[2] Unlike conventional annular Hall thruster, the CHT has smaller surface to volume ratio channel that makes it more convenient for miniaturization and promises reduced plasma-wall interaction leading to erosion of the thruster channel.

All types of Hall thrusters are subject to low frequency oscillations, including breathing oscillations[3] m = 0 (m refers to the azimuthal mode number) caused by an ionization instability, and rotating spoke oscillations[4,5] with m ≥ 1 contributing to anomalous electron cross-field transport. Both types of oscillations may lead to the degradation of thruster performance. The most investigated of these oscillations is the breathing mode,[3] which is mostly an axial mode that is thought to be associated with an ionization instability. The breathing oscillations are observed as discharge current oscillations and can also be seen using high speed images of the background light emission of the working gas. These oscillations are typically low frequency (less than few tens of kHz) and propagate in the axial direction. While extensive investigations both in theory and experiment of the breathing mode have been performed, the underlying physical mechanism generating these instabilities is not yet fully understood, including the breathing mode effects on the ion dynamics.

In order to address the impact of the breathing mode on the ion dynamics, we first describe an heterodyne based laser-induced fluorescence (LIF) technique that allows for probing the ion dynamics while resolving the breathing mode. In fact, we induced plasma disturbances that couple to the intrinsic breathing mode in order to investigate the effects of this mode on the ion velocity distribution function (IVDF). The coupling to the breathing mode is a key in the application of the described diagnostic. More specifically,

we induce coherent breathing oscillations by driving small oscillations of the anode voltage and then using a novel LIF heterodyne approach, a time-resolved (TR) IVDF is obtained. This approach contrasts and complements the photon counting technique for obtaining such time-resolved IVDF as reported in Refs. 6 and 7. Reference 6 obtained the TR-IVDF signal using a photon counting approach while the breathing oscillations are induced. Reference 7, on the other hand, used a transfer function approach to reconstruct the TR-IVDF. Both approaches require long acquisition times to resolve the IVDF as each ion velocity class needs to be acquired with enough statistics to enable the reconstruction.

We propose a new approach that relies on the harmonic decomposition of the IVDF and employs a heterodyne technique to extract all the harmonic components of the IVDF before preforming a reconstruction of the IVDF. This approach is discussed in Sec. III after a brief description of the experimental setup in Sec. II. Section IV describes simulations to compare with experimental observations. Finally, a discussion and summary are provided in Sec. V.

II. EXPERIMENTAL APPROACH

The experiments are performed in a 2.6 cm CHT (see Figures 1(a)–1(c)). The design and detailed description can be found in Refs. 2 and 8. The thruster was operated using xenon propellant with anode flow rate of 2.5 sccm and cathode flow rate of 1.5 sccm. The background pressure during thruster operation was about 5.1×10^{-5} Torr. The back magnetic coil current was 0.6 A and the front magnetic coil current was 1.27 A in "direct" configuration. A 0.25 A keeper current was run between cathode emitter and keeper, together with a 12 A heating current to stabilize the hollow cathode performance. When the discharge voltage was set to be 225 V, the thruster exhibits strong breathing oscillation at about 11.5 kHz.

To investigate the effect of the breathing oscillations on the IVDF, we developed a coupling circuitry in two iterations.
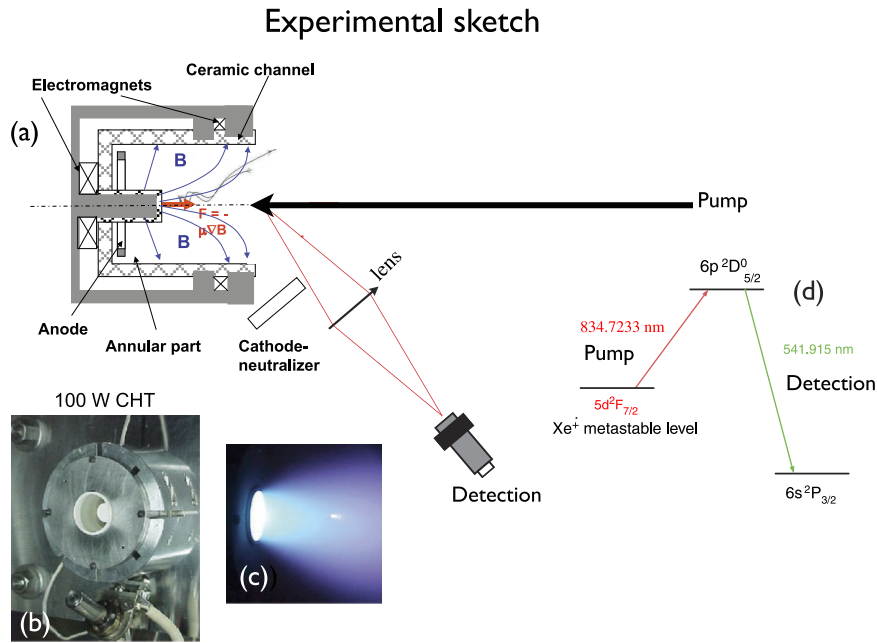
Experimental sketch

FIG. 1. (a) Schematics of the cross section of the CHT and LIF diagnostics. (b) Photograph of the CHT. (c) Photograph of plasma ejection from the CHT. (d) Three level LIF scheme used in this paper.

The first iteration of the circuitry provided square wave modulations of the discharge voltage, which in turn induces coherent oscillations in the plasma. The second, more refined iteration, produces a sinusoidal modulation. In driving the breathing mode, the two iterations generated similar coherent modulations at the fundamental frequency. Other nonlinear effects occur at higher frequencies when the square wave modulation was used. The driving frequency ranges between 5 and 20 kHz with a modulation amplitude ranging between 3 and 30 V. Note that this modulation is applied to the anode, which is already at 220 V. Varying the modulation frequency provides evidence that coupling to the natural breathing oscillations is achieved. Such coupling occurs at around 12 kHz, which corresponds to the intrinsic breathing mode. This approach has been also performed in Ref. 6, where the electron beam was modulating through injection of a little amount of power (a few W) into the cathode system.

To resolve the IVDF, we utilize the LIF diagnostic technique. A tunable diode laser is used to pump the $5d^2F_{7/2}$ Xe$^+$ metastable level to $6p^2D^0_{5/2}$, as shown in Figure 1(d). The laser beam is aligned perpendicular to the thruster exit plan. The collection of LIF photons is performed at $\sim70°$ with respect to the laser beam. The collected signal was detected using a photo-multiplier tube (PMT) with a 10 nm interference filter centered at 541 nm. This setup is used to implement a novel
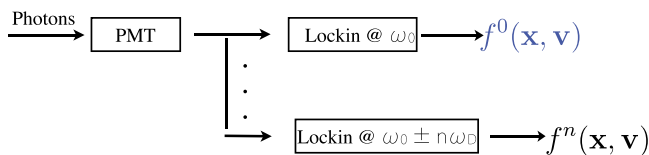

FIG. 2. A sketch of the LIF heterodyne decomposition of IVDF. The photons are detected using a photomultiplier tube (PMT) that can be fed to multiple lockin amplifiers. The signals at various frequency can, in principle, be determined. These signals represent the various components of IVDF.

approach for determining the time-dependent ion distribution based on a heterodyne technique.

III. HETERODYNE-BASED APPROACH

A. Harmonic decomposition

This approach was initially motivated by the need to determine the impact of the rotating spokes on the IVDF. Instead of probing the rotating spokes, this first implementation focused on the breathing modes. As an initial step, we start by the harmonic decomposition of the IVDF as follows:

$$
\begin{aligned}
f(t,\mathbf{x},\mathbf{v}) &= f^0(\mathbf{x},\mathbf{v}) \\
&+ \mathcal{R}e\left[\sum_{n>0} f^n(\mathbf{x},\mathbf{v})\exp(-in\omega_D t + i\theta_n(\mathbf{x},\mathbf{v}))\right].
\end{aligned}
$$

Here, ω_D indicates the modulation in the plasma and θ_n represents the associated phase shift. This modulation could be either intrinsic or imposed by means of external excitation. The equation above describes the time-dependent IVDF due to the coherent oscillations present in the plasma. To validate this decomposition, we focus on driven oscillations which could be extended to intrinsic oscillations. This is left for future work.

In the remainder of this work, we choose to consider the breathing mode. This mode is ubiquitous to most Hall thruster plasmas and can be driven by means of external modulations of the anode (similar approach has also been described in Ref. 6). More specifically, the anode voltage is modulated to induce a breathing mode at $\omega_D = 12$ kHz. This can readily be shown by varying the driving frequency and observing the plasma light emission for maximum fluctuations, which represents the optimum coupling with the background plasma.

To extract the different components of the IVDF, we implement the equation above. We mix $f(t,\mathbf{x},\mathbf{v})$ with the
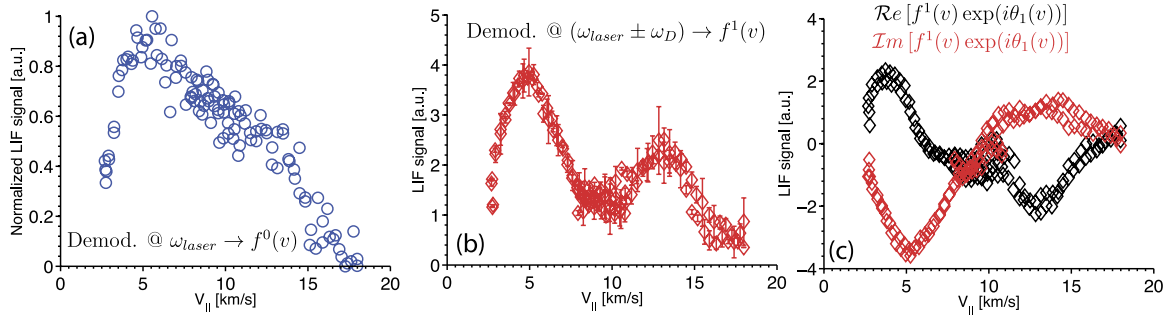
FIG. 3. Measurements of the first two components of the IVDF. (a) The LIF signal demodulated at ω_{laser} yields $f^0(\mathbf{v})$. (b) This component represents $f^1(\mathbf{v})$. (c) The real and imaginary parts, as detected by the lockin amplifier, are displayed.

modulation of the laser beam (ω_{laser}). Note this approach is typically used for most LIF systems and the mixing is usually folded into the lockin detector. Given that this heterodyne approach is used to determine the time averaged IVDF, we extend it to determine the higher orders IVDF. More generally, such extension yields $f^n(\mathbf{x}, \mathbf{v})$ when the mixing is performed at $\omega_{laser} \pm n\omega_D$ ($n \geq 0$). Figure 2 sketches this LIF heterodyne scheme where the various components of the IVDF are displayed.

Figure 3(a) displays the demodulated component at ω_{laser}, which represents the zeroth order component of the distribution $f^0(\mathbf{v})$. Note that this component is different for the time-averaged IVDF but represents the zeroth order component of the IVDF. Figure 3(b) displays the first order component and Figure 3(c) represents the real and imaginary parts of $f^1(\mathbf{v})$ from which the phase can be determined for the full reconstruction of the time-dependent IVDF as shown in Figure 4. It is worth noting that the higher order ($n \geq 2$) components are weak (when sinusoidal modulations are applied) and do not contribute in the reconstruction. In fact, Figure 5 displays the second order component $f^2(x, v)$, which clearly shows a large scatter in the phase indicative of the measurements of the second order component being in the noise level. This suggests that the higher order ($n \geq 2$) perturbations have little impact on

the ion dynamics via the IVDF. Overall, this harmonic based reconstruction bears some similarity with the photon counting based time-dependent IVDF shown in Figure 26 of Ref. 9.

B. Characterization

In order to further characterize the harmonic based reconstruction, efforts have been made to change the modulation waveform of the anode (ω_D) from a square to a sinusoidal waveform to reduce any nonlinear coupling between harmonics. Figure 6(a) displays the time-averaged contribution of IVDF when 207 V and 233 V are applied to the anode. These voltages represent the peak and trough of the sinusoidal waveform. In other words, when the sinusoidal waveform is applied, the voltage swings between 207 and 233 V dc. We set the anode voltages to describe and obtain $f^0(\mathbf{v})$ as shown in Figure 6(a). In this figure, the peak distribution is slightly shifted at the applied voltages. This approach suggests that the applied voltages appear to shift the IVDF along the velocity axis, which is reminiscent of a sloshing motion.
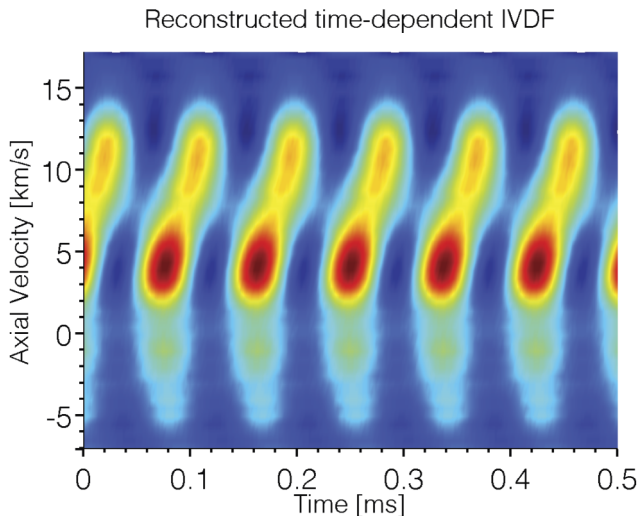

FIG. 4. The time resolved IVDF reconstructed from all the first two components of the harmonic decomposition of the IVDF.
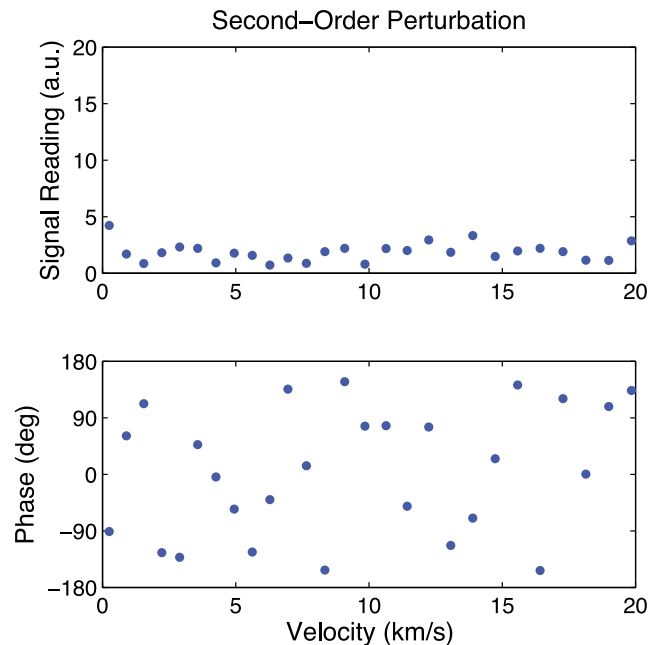

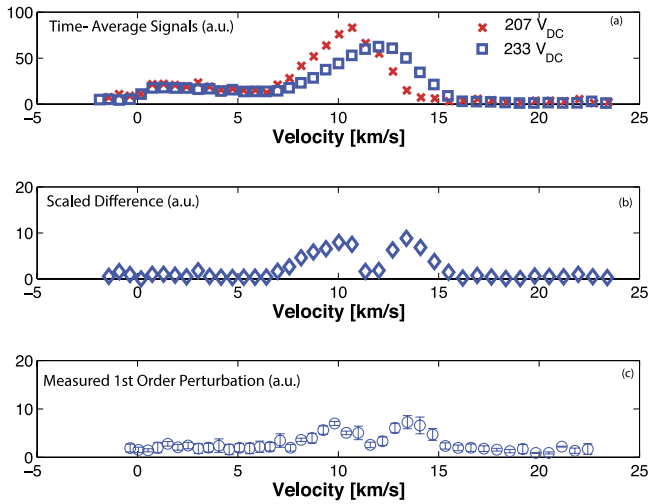FIG. 5. The second order perturbation $f^2(x, v)$.

FIG. 6. Bias voltage induced sloshing of the IVDF. (a) Measured IVDF for two different voltage settings on the anode. (b) Scaled difference of the two sets of the IVDF. (c) An example $f^1(\mathbf{v})$ that highlights the double peaks.

FIG. 7. Time-evolution of the IVDF in (a) relative of the discharge current phase (b).

To recover the double-hump $f^1(\mathbf{v})$ of the IVDF, we scaled and performed a difference between the two distributions in Figure 6(a). The resulting difference is shown in Figure 6(b). This double-hump function bears some similarity with the first order perturbation $f^1(\mathbf{v})$ of the IVDF as displayed in Figure 6(c). While this equivalence between the scaled difference and $f^1(\mathbf{v})$ is difficult to assess, it is clear that the time averaged IVDF $f^0(\mathbf{v})$ appears to slosh back and forth between two mean velocities induced by the peak voltages.

Further assessments of the sloshing of the IVDF are performed by effectively monitoring the discharge current and observing the IVDF relative to the discharge current phase. For such observation to be accurate, an absolute phase, unlike that determined by the lockin amplifier, needed to be provided. Recall that the time-averaged IVDF is the output of the lockin amplifier, which also outputs a relative phase. To determine the time evolution of the IVDF, measurements of the absolute phase are required. This was determined by establishing the zero phase point in time between the modulated laser beam waveform and the driver modulation waveform, which is determined when the peaks of the two waveforms match at t_{ref}. The offset between t_{ref} and the reference signal of the lockin amplifier can then be translated into a phase shift offset which is added to the lockin phase to obtain the absolute phase shift. Such absolute determination of the phase enables the quantification of the IVDF relative to global thruster parameters such as the discharge current, as displayed in Figure 7. In this figure, the IVDF is plotted at various phases of the discharge current, once again suggesting that the IVDF is sloshing during the discharge current evolution. Motivated by this sloshing, simulations are performed to investigate the potential physical parameters that can be extracted from $f^1(\mathbf{v})$.

IV. SIMULATIONS AND COMPARISON WITH EXPERIMENT

To further understand the physical quantities encoded in the different components of the IVDF, we assume that the $f^1(\mathbf{v})$ of the IVDF is sloshing due to the applied
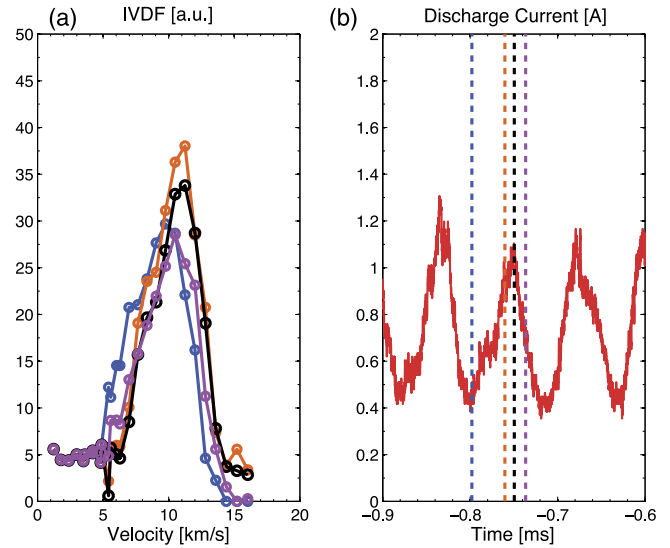
modulation (ω_D) of anode. Note this assumption is motivated by the scaled difference approach illustrated in Figure 6. In addition, this is the only key assumption in the model we describe below. The model we present below utilizes the observations described above (as shown in Figures 6 and 7) to reproduce the first order component. For instance, by changing the voltage in harmonic way, one expects modulation of the IVDF, which in turn can affect the overall density. Furthermore, the assumptions can be modeled by recognizing that these modulations yield small kicks to the plasma $\delta v = \frac{qE}{\omega_D m}$ around a velocity v_0, which yield an effective velocity $v_0 + \delta v \sin(\omega_D t + \varphi)$. Here, φ is an arbitrary phase, E is the local electric field, and m and q are the mass and electric charge, respectively. The perturbation induced IVDF can then be represented as a convolution of a Gaussian and the kicks as $\mathcal{A}(t) \exp(-(v(t) - v_0)^2/(2v_{th}^2))$. In the analysis below, $\mathcal{A}(t) = \exp(-(t/\tau - \Theta(t/\tau))/(\tau_{Decay}/\tau))$. Here, Θ is defined
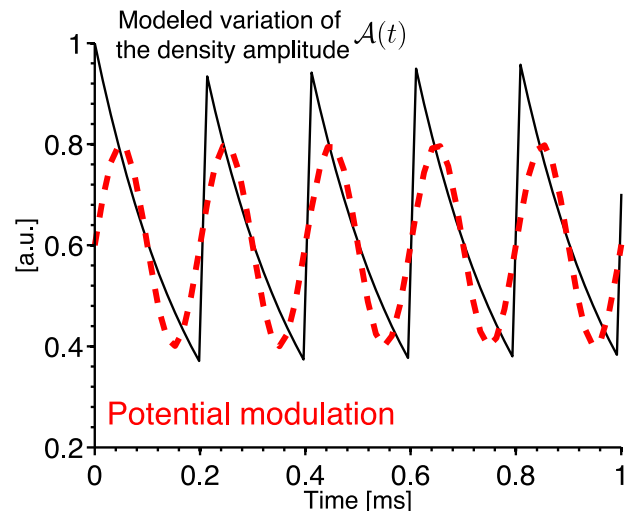

FIG. 8. Amplitude modulation modeling the motion of the ionization front is in solid line. The applied modulation of the anode is shown in a dashed red line.
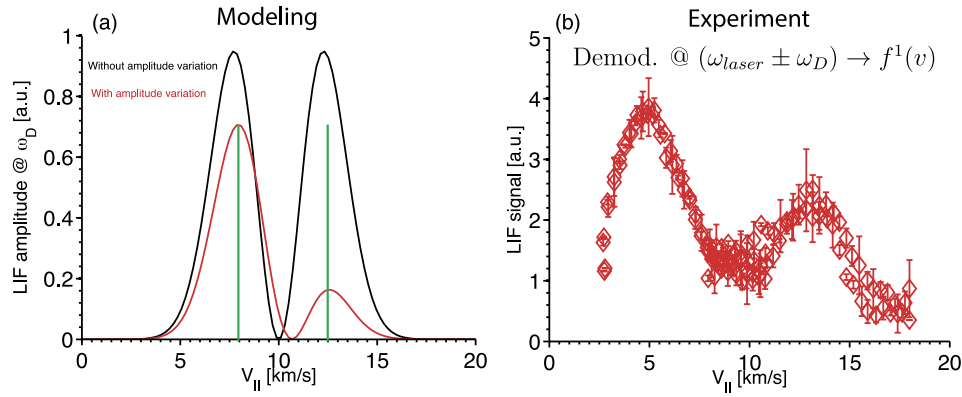
FIG. 9. Experiment-modeling comparison. (a) The left panel shows the model $f^1(\mathbf{v})$ with (red) and without (black) amplitude modulation. The vertical green lines illustrate the peaks' separation. (b) The right panel shows the measured $f^1(\mathbf{v})$. The modeling using the amplitude variation better captures the asymmetry of the peaks on $f^1(\mathbf{v})$.

as the integer part, and τ and τ_{Decay} define, respectively, the modulation period time and the decay of the amplitude between each modulation cycle.

Figure 8 displays the amplitude modulation $\mathcal{A}(t)$, where $\tau_{Decay}/\tau = 1$. This amplitude's modulation is in phase with the potential modulation as illustrated by the red dotted line in Figure 8. The time varying IVDF is then Fourier decomposed and $f^1(\mathbf{v})$ is obtained by extracting the component at ω_D as displayed in Figure 9(a). In this figure, the IVDF at ω_D for the case of constant amplitude ($\mathcal{A}(t) = 1$) as well as with varying amplitude is shown. This figure suggests that to recover similar trends as in the experiment (see Figure 9(b)), one needs to consider a varying amplitude $\mathcal{A}(t)$. The varying amplitude $\mathcal{A}(t)$ clearly yields an asymmetry in the peaks. In addition to the peaks' amplitude asymmetry, the peaks' separation is associated with the δv kicks. This separation is marked by the two green vertical lines in Figure 9(a). Overall, both the kicks δv and the amplitude variations $\mathcal{A}(t)$ provided the means to recover the experimental results. Here, $\mathcal{A}(t)$ captures the back-and-forth motion of ionization front. This approach attempts to mimic the derived model of Ref. 10 in which the slow progression and the fast recession of the ionization front are investigated.

For a given amplitude $\mathcal{A}(t)$, Figure 10 displays the dependence of the peaks' separation as a function of the kicks δv. From the scaling on this figure, one can determine the local potential E necessary to yield the observed peaks' separation. More specifically, given the observed peaks' separation in Figure 3(b), one can determine the kicks δv required. For the specific case of Figure 3(b), such kicks correspond to an amplitude modulation of 30 V peak-to-peak. In addition to providing the time-dependent IVDF, measurements of the harmonics of the IVDF can provide information on the local potential and the displacement of the ionization front motion. The physics of this ionization front motion will be investigated in future publication.

We perform a scan of the motion of the ionization front where this motion is modeled using the decay time relative to the modulation period τ_{Decay}/τ and studied its impact on the peaks' amplitude of $f^1(\mathbf{v})$. As shown in the left panel of Figure 11, the time evolution of the amplitude $\mathcal{A}(t)$ is displayed for three cases of decay time. This variation

accounts for the effective ionization front motion as seen by the measurement volume. The impact of this decay time can readily be observed as a variation of the peak amplitude as displayed in the right panel of Figure 11. This scan in τ_{Decay}/τ suggests that for $\tau_{Decay} = 200\ \mu s$, one can recover the first order component of the IVDF as shown in Figure 3(b). Overall, the simulations show that using a simple approximation of the phenomena modeled as sloshing the IVDF, one can recover qualitatively the measured first order component of the IVDF. Applications of this harmonic based decomposition of the IVDF for the investigation of the ubiquitous spoke phenomena in Hall thrusters can now readily be tackled. In fact, initial measurements were conducted and reported the feasibility of the proposed measurements for azimuthal oscillations[11] and will be the subject of future publications.

V. DISCUSSION AND SUMMARY

We presented a novel harmonic based time-dependent reconstruction of the IVDF in a Hall thruster. The IVDF was obtained using the heterodyne detection of the LIF
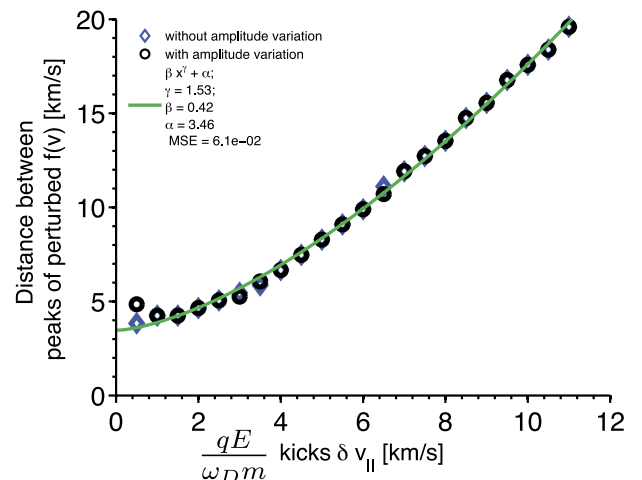

FIG. 10. Scaling of the kicks δv as a function of the peaks' separation. Both with and without amplitude variations of the IVDF are overlaid. A fit $\beta x^\gamma + \alpha$ of this scaling is also displayed.
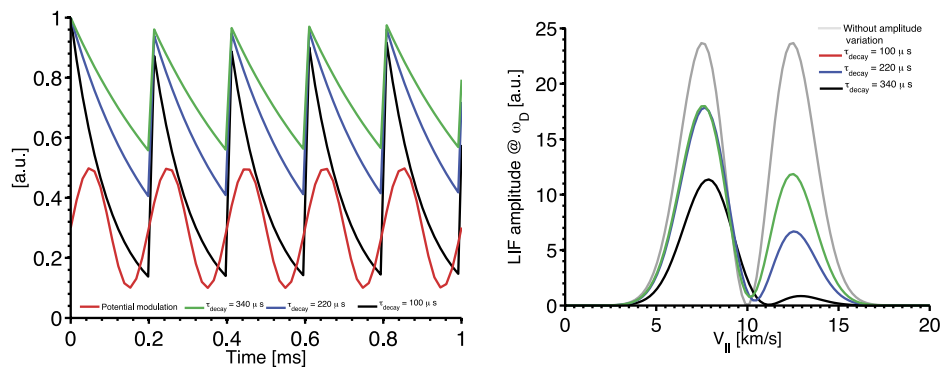
FIG. 11. Impact of the amplitude decay time (τ_{Decay}) on IVDF peaks' amplitude variation. The left panel shows the various amplitude variations with different decay times. On the same plot, the anode potential modulation is indicated. The right panel shows $f^1(\mathbf{v})$ for three different decay times, in addition to the IVDF without amplitude variation.

signal in Xe II. Characterization of this new approach was performed using an external excitation of the breathing mode as an initial approach and will be extended to other intrinsic instabilities of Hall thrusters. Note that Ref. 12 has shown that the behavior of the current and IVDF is similar to natural breathing oscillations as long as the driving amplitude is small (i.e., in the linear regime). Given the similarity in current and IVDF behavior between driven and intrinsic breathing mode, we used the driven breathing mode approach to demonstrate this novel heterodyne-based time-resolved IVDF using LIF.

The reconstruction based on the various harmonics of the IVDF was shown to be similar to other photon counting approach for the time resolved IVDF pioneered by Mazouffre[9] and the work of Durot[7] using the transfer function. Note that another approach using comparator to determine the time synchronization between the fluorescence signal and thruster discharge was recently implemented by Young.[13] Note that direct comparison between all these approaches has yet to be performed. While the photon counting and the heterodyne approaches rely on coherent oscillations present in the CHT, the transfer function appears to be capable of being extended to include incoherent oscillations. Experiments have been undertaken to compare this approach with the photon counting approach most widely used in the Hall thruster community. Unfortunately, the photon counting approach in our device was not successful, mostly due to thermal drifts. Note that the photon counting requires acquisitions of many minutes to reconstruct the full distribution. The thermal drifts tend to change the IVDF during the acquisition in the CHT. The heterodyne approach, however, remains immune to these drifts mainly because the IVDF velocity sweep takes less than 10 min, during which there are no thermal drifts, and therefore, the CHT is stationary.

In addition to the characterization, analysis of the first order component was performed using a simple model that considers kicks in velocity space δv and the amplitude variations representing the back-and-forth motion of the ionization front. This simple model enabled the qualitative agreement with experiment results. One of the main advantages of this approach is the rather fast acquisition that is immune to thermal drifts of drifts in long (~1 h) transient operation typical to Hall thrusters.[14]

Finally, the heterodyne approach to time-resolve the IVDF was validated. This approach can, in principle, be extended to intrinsic oscillations so long as the oscillations are quasi-periodic. Overall, driven coherent oscillations can provide the means to further understand the breathing mode physics via the ion dynamics. For future work, the method will be extended to the intrinsic breathing mode. In addition, future modifications of this system will be made to better assess the coherent spoke instabilities.

[1] M. Martinez-Sanchez and J. E. Pollard, J. Propul. Power **14**, 688 (1998).
[2] Y. Raitses and N. J. Fisch, Phys. Plasmas **8**, 2579 (2001).
[3] J. P. Boeuf and L. Garrigues, J. Appl. Phys. **84**, 3541 (1998).
[4] J. B. Parker, Y. Raitses, and N. J. Fisch, Appl. Phys. Lett. **97**, 091501 (2010).
[5] M. Sekerak, B. Longmier, A. Gallimore, D. Brown, R. Hofer, and J. Polk, IEEE Trans. Plasma Sci. **43**, 72 (2015).
[6] J. Vaudolon, L. Balika, and S. Mazouffre, Rev. Sci. Instrum. **84**, 073512 (2013).
[7] C. J. Durot, A. D. Gallimore, and T. B. Smith, Rev. Sci. Instrum. **85**, 013508 (2014).
[8] A. Smirnov, Y. Raitses, and N. J. Fisch, J. Appl. Phys. **92**, 5673 (2002).
[9] S. Mazouffre, Plasma Sources Sci. Technol. **22**, 013001 (2013).
[10] S. Barral and Z. Peradzynski, "A new breath for the breathing mode," presented at the 31st International Electric Propulsion Conference, University of Michigan, Ann Arbor, Michigan, USA, 20-24 September 2009.
[11] Y. Shi, A. Diallo, S. Keller, and Y. Raitses, "Driving Low Frequency Azimuthal Mode in Cylindrical Hall Thruster with a Segmented Anode," presented at the 33rd International Electric Propulsion Conference (IEPC-2013), George Washington University, Washington, D.C., USA, 6–10 October 2013.
[12] S. Keller, Y. Raitses, and A. Diallo, "Driving Low Frequency Breathing Oscillations in a Hall Thruster," in 50th AIAA/ASME/SAE/ASEE Joint Propulsion Conference (AIAA, 2014).
[13] C. V. Young, A. Lucca Fabris, and M. A. Cappelli, Appl. Phys. Lett. **106**, 044102 (2015).
[14] R. R. Hofer and R. S. Jankovsky, "The Influence of Current Density and Magnetic Field Topography in Optimizing the Performance, Divergence, and Plasma Oscillations of High Specific Impulse Hall Thrusters," in Proceedings of the 28th International Electric Propulsion Conference, (Electric Rocket Propulsion Society, Cleveland, 2003), IEPC-2003-142.